PSFC/JA-10-67

Measurement of wakefields in a 17 GHz photonic bandgap accelerator structure

Marsh, R.A., Shapiro, M.A., Temkin, R.J., Smirnova, E.I.*, DeFord, J.F.**

* Los Alamos National Laboratory, Los Alamos, NM 87545
** Simulation Technology & Applied Research, Inc., Mequon, WI 53092

2010

Plasma Science and Fusion Center
Massachusetts Institute of Technology
Cambridge MA 02139 USA

This work was supported by the Department of Energy, Division of High Energy Physics Contract no. DE-FG02- 91ER40648.

Measurement of Wakefields in a 17 GHz Photonic Bandgap Accelerator Structure

Roark A. Marsh[a,b], Michael A. Shapiro[a], Richard J. Temkin[a], Evgenya I. Smirnova[c], John F. DeFord[d]

[a] *Plasma Science and Fusion Center, Massachusetts Institute of Technology, Cambridge, MA 02139*
[b] *Lawrence Livermore National Laboratory, Livermore, CA 94550*
[c] *Los Alamos National Laboratory, Los Alamos, NM 87545*
[d] *Simulation Technology & Applied Research, Inc., Mequon, WI 53092*

Abstract

We report the experimental measurement of wakefields in a 17.14 GHz metallic photonic bandgap accelerator structure and its comparison with theory. Damping of wakefields is a critical issue in the next generation of high gradient electron accelerators, and photonic bandgap (PBG) structures have unique properties for suppressing and damping wakefields. In the experiments the wakefields were generated by passing an 18 MeV electron beam through the six cell 17.14 GHz structure. The wakefield radiation was measured at two locations: the structure output port, and at a window viewing port located at the side of the structure. The electron beam consisted of a train of bunches spaced at 17.14 GHz, so that only radiation at 17.14 GHz and its harmonics was observed. Wakefields at up to the fifth harmonic (85.7 GHz) were detected by a heterodyne receiver system. The wakefield power levels were measured at 17 and 34 GHz for average currents between 20 and 300 mA. The results were compared with full wakefield simulations using the code *ANALYST*. The measured power level at 17 GHz was in excellent agreement with the theoretical estimate, but the measured power at 34 GHz was significantly lower than the theoretical estimate. At both 17 and 34 GHz the measured power level increased as the beam current squared, as expected from theory. The experimental results demonstrate the weak excitation of high order mode wakefields in a photonic bandgap structure.

Key words: photonic band gap, higher order mode damping, wakefields
PACS: 41.20.-q, 41.60.-m, 52.70.Gw

1. Introduction

Photonic crystals are an appealing theoretical starting point for a damped structure. The frequency dependent properties of photonic crystals make it possible to form the confining wall of an accelerator structure such that a fundamental, operating mode is confined, but higher order modes (HOMs), which are of higher frequency are not. The use of a metallic photonic bandgap (PBG) structure as an accelerator was first proposed based on a square metallic lattice in [1]. A structure with a triangular lattice has improved symmetry for accelerators and good agreement was observed between network analyzer measurements and *HFSS* simulations [2]. A six cell traveling wave structure has also been built, based on this first design [3]. The PBG structure demonstrated acceleration using a photonic structure for the first time [4]. The HOM damping properties of the structure were not studied during those experiments. Simulations of the structure did in fact reveal HOMs confined in the structure, but these were interpreted as being confined by the metallic outer wall used in simulation and absent in the experiment [3].

Wakefield damping is an important consideration in accelerator structure design. A number of innovative solutions have been suggested in order to provide damping sufficient for the next generation of both high energy linear accelerators and high brightness light sources. These solutions include waveguide damping on the cavity itself [5], on the beam pipe [6], slotted irises [7], HOM damping couplers [8], choked mode structures [9], dielectric PBG structures [10] and both square [1] and triangular lattice [2] metallic PBG structures.

In order to quantitatively assess damping in any accelerator structure, structures must eventually be built, and can then be analyzed in both cold and hot tests. Cold testing methods can involve network analyzer bench measurements, including port excitation, bead pull, or wire excitation [11]. Hot testing involves a direct measurement of wakefields excited by a beam. This can be done using a single high charge bunch or a train of bunches, and measuring radiated power [12, 13]; or by probing the wake potential using the adjustable separation of an exciting and witness bunch [14].

The general transverse wake potential, $W_\perp$, can be written as a sum over cavity modes, n, and a function of the mode kick factor, $k_{\perp n}$, mode frequency, ω_n, mode quality factor, Q_n, and the distance from the exciting charge, s, as shown in Eq. 1 [15].

$$W_\perp(s) = \sum_n 2k_{\perp n} e^{-\frac{\omega_n s}{2Q_n c}} \sin\frac{\omega_n s}{c} \tag{1}$$

Wakefield damping results in a reduced wake potential, so that bunches subsequent to the exciting bunch are not significantly disrupted. Damping can be achieved by reducing the magnitude of the potential, but also by increasing the loss of unwanted modes, so that they damp rapidly in time or bunch separation.

Email address: marsh19@llnl.gov (Roark A. Marsh)

Early theoretical research indicated that PBG structures have no HOMs, and so the sum in Eq. 1 would contain no modes [3]. Higher order modes, unconfined by the band gap, were thought to propagate out through the structure and be of little or no significance. This paper investigates the detailed properties of these HOMs through simulations and experiments to understand the nature of HOMs in PBG structures. HOMs exist in PBG structures as lossy modes that have low Q due to high loss into the PBG lattice. Because HOMs exist, they must be understood and damped for PBG structures to be viable accelerator structures.

Following a demonstration of acceleration, the specific wakefield damping parameters of the structure are of interest. Experiments are reported in this paper, with preliminary results reported in [13, 16] to directly observe wakefield radiation produced by passing an electron beam through the unpowered six cell structure. In order to predict the power lost by the beam into the structure, *HFSS* simulations were performed to probe the properties of various PBG HOMs, after [17]. Time domain simulations were also performed to calculate directly the wakefields excited by a bunch train transiting the structure using the STAAR code *ANALYST* [18, 19].

In this paper we report measurements of beam induced wakefields in a PBG accelerator structure. The wakefield power is measured with calibrated diode detectors and compared with numerical wakefield simulations. The structure of this paper is as follows: the PBG structure is described more fully in both simulations and cold test in Section 2, the experimental setup and results are described in Section 3, and the paper is concluded in Section 4.

Rod radius	a	1.04 mm
Rod spacing	b	6.97 mm
Iris thickness	t	1.14 mm
Iris diameter	d	4.32 mm
Cavity length	L	5.83 mm
TM_{01} frequency	f_{rf}	17.14 GHz

Table 1: Dimensions and design properties of the six cell PBG accelerator structure. Lettered abbreviations represent the dimensional labels used in the schematic of Fig. 1.

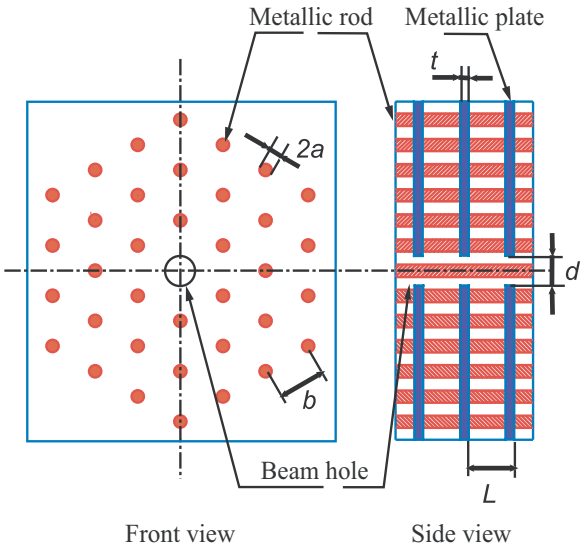

Figure 1: Schematic of the six cell PBG accelerator structure. A PBG lattice is formed by a triangular lattice of cylindrical metallic rods; one rod is removed from the center to form a defect which confines the TM_{01} operating mode. Dimensions for labels are given in Table 1.

2. Theory and Cold Test

Understanding wakefields in PBG structures requires a balance of theory predictions and experimental observations. PBG structures are especially prone to modes which appear to be simulation artifacts. This section discusses theory predictions for wakefields in the six cell PBG structure. Direct wakefield calculations have been made using the STAAR code *ANALYST* [18, 19]. Eigenmode calculations using *HFSS* have also been used to understand HOMs in PBG structures.

2.1. *Introduction*

The PBG accelerator structure used for these experiments was designed, built, tuned, and tested as previously reported [3, 4]. The PBG structure is made up of a triangular lattice of cylindrical rods, with a one rod defect; end plates are flat metallic plates with beam holes, or irises. Design parameters are summarized in Table 1 as represented in Fig. 1. Wakefield measurements and simulations refer to the locations shown in Fig. 2.

2.2. *Wake Calculations using* ANALYST

Calculations of wakefields generated by a train of 17.14 GHz bunches transiting the six cell PBG accelerator structure were carried out using the *ANALYST* parallel finite-element software package developed by Simulation Technology & Applied Research (STAAR) [18, 19]. For this work the time-domain field modeling component of *ANALYST* (called *TD3P*) was used. It uses a high-order adaptive finite-element method with an implicit time-step to accurately compute time-domain fields on unstructured tetrahedral meshes of widely varying element size. *TD3P* was used to simulate a train of Gaussian electron bunches traveling at the speed of light along the axis of the PBG structure. The bunch spacing was chosen to be 17.49 mm, giving a 17.14 GHz period corresponding to the spacing used in the experiments. The bunch length was a factor of 10 larger than that used in the experiment in order to minimize meshing requirements and numerical noise in the solution.

The wake calculations were performed with field monitors at both the structure input and output ports, using a length of simulated waveguide to temporally isolate waveguide terminations so that the resulting time-domain signals correspond to matched terminations. The field monitors are polarized in the same way the detector diodes were in the experiment, to accurately compare power measurements with theory predictions. Fourier transform results are given in Fig. 3. Power is excited coherently at integer multiples of the bunch repetition frequency, which is equal to f_{rf}, 17.14 GHz; peaks are observed

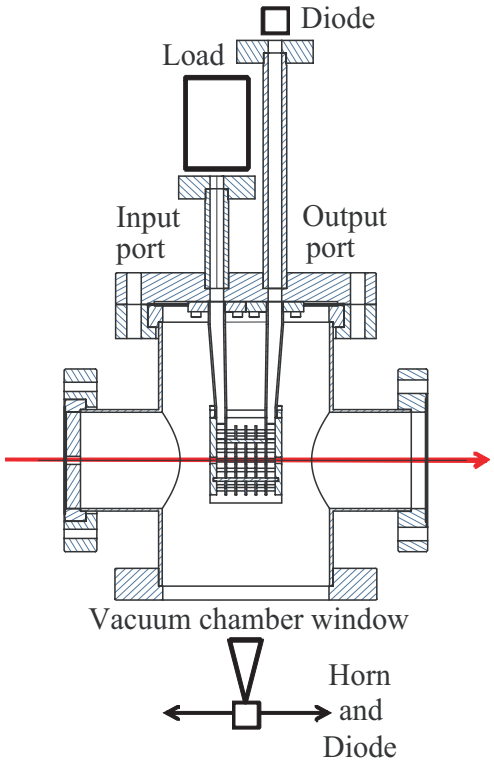

Figure 2: PBG accelerator structure vacuum vessel. The waveguide input and output ports, and the chamber window on the bottom of the vacuum chamber are labeled. The positions of the matched load and diode detectors are shown. The beam path is indicated with a red arrow.

in the spectrum near 17.14, 34.28, 51.42, and 68.56 GHz.

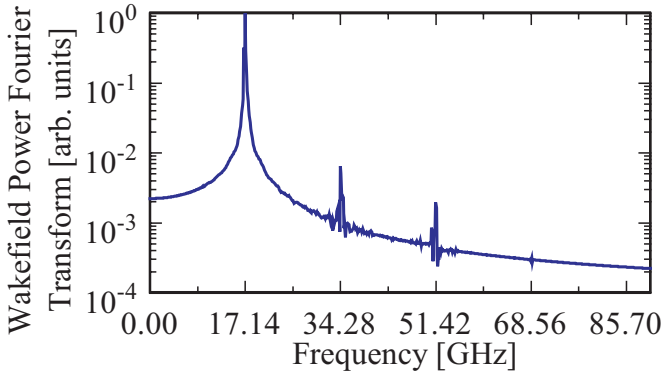

Figure 3: Fourier transform of beam induced wakefield power versus frequency, as calculated using *ANALYST* for a 10 ps bunch length.

The electric field Fourier transform can be used to obtain the ratios of power predicted at different frequencies. The field results are multiplied by the ratio of the Fourier transforms at the specified frequency of the bunch train lengths, in order to extrapolate the results from 10 ps simulations to the experimental Gaussian bunch length of 1 ps. The field numbers are then squared to obtain power figures, and ratios of predicted power are obtained. Observed at the output port, the ratio of 17.14 GHz power to 34.28 GHz power is 620. The absolute power level at 17.14 GHz can be obtained by integrating the field data over the waveguide cross section, predicting 1.5 kW. Combining these figures, 2.4 W of power is expected at 34.28 GHz.

2.3. *Quality Factor Simulations*

Initial simulations showed HOMs confined in the PBG structure that were not localized to the defect, but distributed throughout the structure [4]. It was believed that these HOMs are only confined by the outer metallic boundary, and not by the PBG lattice. As reported in this paper, these modes are not artifacts, but leaky modes with low Q factors.

In order to study the diffractive Q of the HOMs, *HFSS* simulations were run for an outer boundary that more closely resembles that of the experiment, which is open. This was done using a perfectly matched layer (PML). An *HFSS* PML result is shown in Fig. 4; the electric field complex magnitude is shown for the 17 GHz TM_{01} fundamental, a 23.0 GHz dipole mode, and a 34 GHz HOM . The field strength of the HOMs is localized to the lattice, away from the beam, and very high diffractive loss has been observed for these modes, with diffractive Q's on the order of ~100.

To directly compare the effect of different structure losses on the cavity Q, *HFSS* simulations were performed with different boundary conditions. The quality factors associated with the different structure losses are: Q_{ohmic}, and $Q_{diffractive}$, which account for losses from ohmic surface heating, and the open nature of the structure, respectively. These quality factors can be combined using Eq. 2.

$$\frac{1}{Q} = \frac{1}{Q_{total}} = \frac{1}{Q_{ohmic}} + \frac{1}{Q_{diffractive}} \tag{2}$$

Using *HFSS* these quality factors can be calculated independently by turning on or off the different loss channels: Q_{ohmic} can be estimated by simulating a single PBG cell with phased boundaries on the irises, a metallic outer boundary, and ohmic losses; $Q_{diffractive}$ can be estimated by simulating a single PBG cell with phased boundaries on the irises, no ohmic losses, and a PML outer boundary; Q_{total} can be estimated by simulating a single PBG cell with phased boundaries on the irises, a PML outer boundary, and ohmic losses.

According to [15] the power expected in each channel scales inversely with Q. This allows the ratio of power radiated into each channel to be predicted based on the following Q values for the 17 GHz fundamental, and the 23 and 34 GHz HOMs, as shown in Table 2. The 17 GHz mode has minimal diffractive loss, whereas the 23 and 34 GHz HOMs are primarily losing power diffractively. The very low Q HOMs demonstrate the

Mode	Q_{ohmic}	$Q_{diffractive}$	Q_{total}
17 GHz	4500	$2.5 \cdot 10^5$	4400
23 GHz	3500	60	60
34 GHz	3800	60	60

Table 2: Table of Q values for power ratio prediction for 17 GHz fundamental mode, 23 GHz dipole mode and 34 GHz HOM.

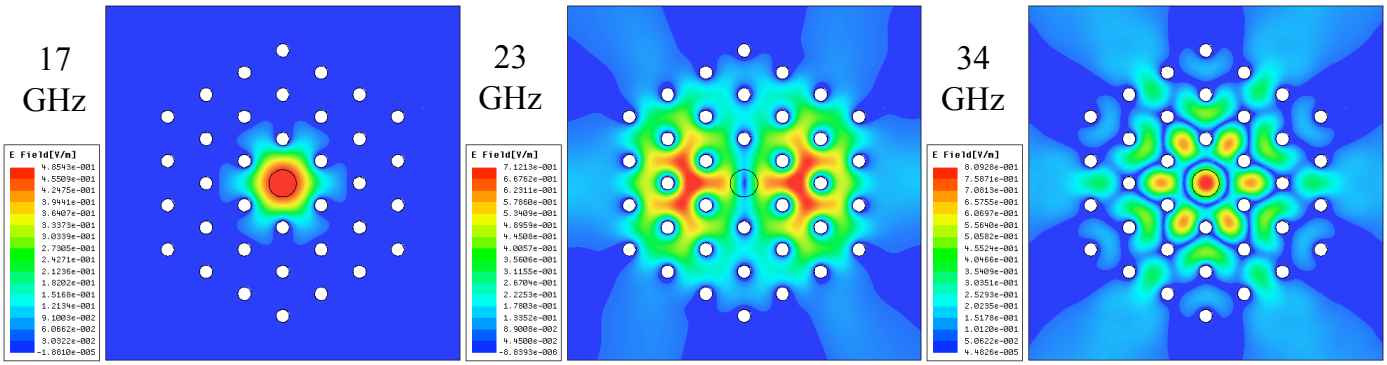

Figure 4: *HFSS* simulations of 17, 23, and 34 GHz modes in one cell of the PBG accelerator structure. Irises and the outer boundary are bordered with PMLs, metallic rods and plates are modeled with ohmic losses. The electric field magnitude is shown in color. Simulation results correspond to the $Q_{diffractive}$ runs as shown in Table 2.

effectiveness of the HOM damping in PBG structures, and predict that most of the power lost in these modes will occur cell by cell, through the open outer boundary of the structure. Some power will couple out of the port, but the modes will not be resonantly built up as they will be for the 17 GHz fundamental mode. The 17 GHz mode will excite a true traveling wave which will couple through the ports, as designed [3].

2.4. Cold Test Measurements

Cold testing of the six cell PBG structure demonstrated the existence and scale of HOM confinement in the structure. The six cell traveling wave structure was connected to an Agilent E8363B Precision Network Analyzer (PNA). The measured S_{21} parameter is shown in Fig. 5 for the open structure without damping, in red in Fig. 5A, and with external damping, in blue in Fig. 5B. The mode structure is rather complex because there are many modes and because of resonances in the PNA SMA cables. The very broad resonance appearing around 17 GHz is in fact the six closely spaced narrow resonances of the six cell traveling wave mode PBG structure. Full range calibration was not done, so that the entire frequency span and dynamic range could be observed in a single pass; for mode identification and precision measurements the full two port calibration was used. Modes were distinguishable in both S_{21} and S_{11} measurements at roughly the following frequencies: 17.14 (fundamental operating band of modes), 23.3, 24.5, 25.7, and 26.7 GHz. The high frequency modes (23–27 GHz) are near the dipole mode frequency of 23.0 GHz. Antennae excitation measurements have been performed to probe the structure of these modes, which exist off-axis and are most easily excited within the bulk of the PBG lattice, as expected given their theoretical field profiles, for example the 23 GHz mode of Fig. 4.

Though the HOMs are excited with very high insertion loss, they are resonant, albeit with very low quality factors. HOMs in PBG structures can be further damped using an external lossy dielectric absorber such as *ECCOSORB* or vacuum-compatible *Ceralloy* or Silicon Carbide. The use of non-vacuum-compatible lossy materials at the outer boundary of the structure in cold test measurement was seen to significantly decrease the observed modes, as shown by the blue S_{21} curve in Fig. 5B. As observed in simulations, lossy material added to PBG structures can dramatically damp HOMs [17, 20].

3. Results

3.1. Experimental Setup

The bunch train used in these radiation experiments was created with the 17 GHz linac manufactured by Haimson Research Corporation and installed at MIT. The parameters of the linac are summarized in Table 3. The linac is powered by a single

rf Frequency, f_{rf}	17.14 GHz
Beam Energy	18 MeV
Bunch Length	1 ps
Average Beam Current	20–300 mA

Table 3: Operating parameters.

high power modulator [21], which was operated at 500 kV, producing one microsecond flat top pulses for both the linac DC thermionic gun, and a 17.14 GHz klystron [22]. Beam current and size are controlled by focusing the beam with solenoidal lenses prior to collimation. The DC beam is bunched prior to linac injection using an rf chopper and prebuncher system [23]. The system was operated in a long pulse mode, in which the DC beam is primarily prebunched, with low chopper power operating only to remove a low energy tail from the bunch; this produced 1 ps bunches, as verified using a circularly polarized beam deflector bunch length diagnostic [24, 25]. The linac is a constant gradient traveling-wave structure consisting of 94 cells operating in a $2\pi/3$ mode, providing a beam energy of 18 MeV. An rf pulse length of 100 ns corresponds to a bunch train of ~40 ns because of the 60 ns fill time of the accelerator structure. A toroidal lens follows the linac where the beam is focused to an emittance limited spot size of 1 mm. This size was verified by beam interception measurements. The beam was then passed through the PBG experimental chamber shown in Fig. 2, and into a Faraday cup for current measurement and beam dump.

The six cell PBG structure is housed in a stainless vacuum vessel on the beam line, shown schematically in Fig. 2. A

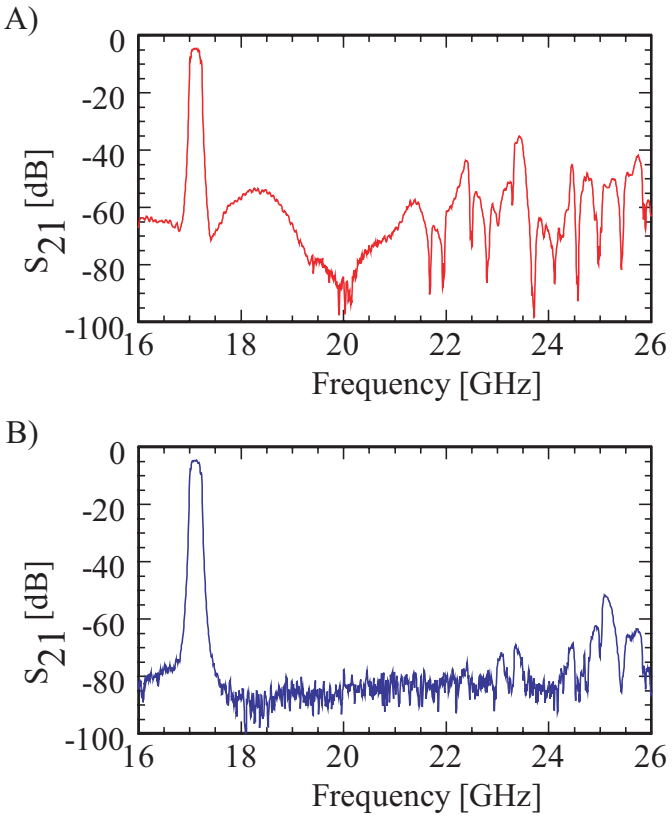

Figure 5: Six cell metallic PBG accelerator structure uncalibrated S_{21} measurement. A) is measured S_{21} in red without damping, B) is measured S_{21} in blue with external damping. Modes are observed at: ~17, and 23–27 GHz. 6 modes are marginally resolved at 17 GHz, giving the resonances a broad appearance.

fused quartz window was installed on the bottom of the vacuum chamber housing the PBG structure, as labeled in Fig. 2, so that radiation could be observed leaking out of the open PBG structure. The input and output couplers, as labeled in Fig. 2, were mounted with vacuum windows so that observations could also be made of radiation coupling out of the structure via the input and output coupler ports. During these wakefield measurements, no microwave power was injected into the structure.

Two sets of diode detectors were used, at both Ku (12–18 GHz) and Ka (26–40 GHz) bands. They were calibrated using their respective power heads and meters. The horns, waveguide, adapters, attenuators and vacuum windows used were calibrated over their respective frequency ranges using an E8363B Agilent PNA; this allowed power to be measured on an absolute scale. A heterodyne receiver was used to look at the frequencies of the observed radiation. This heterodyne system consisted of an 8–18 GHz YIG local oscillator and a 2–18 GHz double balanced mixer. Wavemeters and waveguide filters were also used to verify the observed frequency content of the wakefields.

3.2. *Experimental Results*

Radiation is expected to scale quadratically with bunch charge [15]. Wakefield scaling with current was observed as the average current was varied from 20–300 mA, corresponding to a bunch charge in the range of 1–18 pC. Wakefield measurements were made as functions of beam position and current; Table 4 shows a summary of experimental measurements and theoretical predictions for the absolute power, for an average beam current of 100 mA.

	Experiment [Watts]	*ANALYST* [Watts]
17 GHz	1.46×10^3	1.5×10^3
34 GHz	0.24	2.4

Table 4: Summary of power measurements of output port diode: frequency of observed wakefields, fully calibrated power level detected for 100 mA average beam current, and theory predictions.

Excellent agreement has been observed at 17 GHz between measurements made on the output port with a matched input port, and the corresponding theory predictions from the prediction of *ANALYST* from Sec. 2.2. Fig. 6 displays absolute power measurements and the theory prediction. The average current error is measured as shot to shot variation. The power error is calculated as a combination of statistical variation, calibration systematic errors, and beam current error.

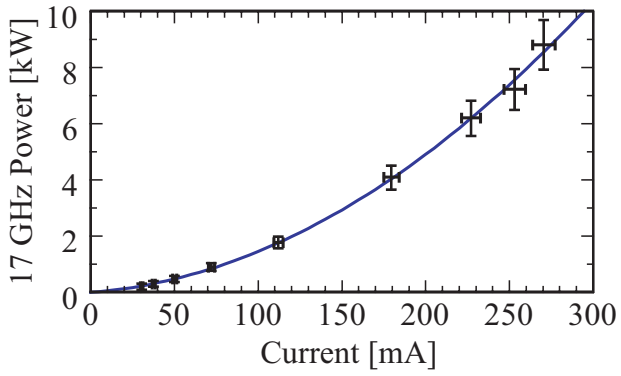

Figure 6: Power observed on output port with matched input port, at 17 GHz, versus current. Theory prediction shown in blue with data given as black bars.

Results for the 34 GHz (Ka-band) diode detector observing on the output coupler port are shown in Fig. 7. Very good agreement is obtained with a quadratic fit, with a small error arising from both the statistical diode signal variation and shot to shot current fluctuation. The absolute value of the power measured at 34 GHz for 100 mA beam current is compared with theory in Table 4. The *ANALYST* prediction for the 34 GHz power is an order of magnitude higher than the measured value. This is a large discrepancy and the explanation is not entirely clear at this time. The wakefield simulations have some inherent error, and demonstrate some sampling variation over the waveguide cross-section. This numerical noise may be the source of some of the discrepancy between theory and experiment. The experimental systematic error at 34 GHz is also relatively large. Power generated at 34 GHz in the structure must transit through overmoded waveguide and a window to reach the Ka-Band detector. The 34 GHz power will evolve into a mixture of higher order waveguide modes during that transmission. Some of these modes will

not couple well to the Ka-Band detector. The window, which is matched at 17 GHz, is overmoded and not well matched at 34 GHz. Although we attempted to account for these effects in our calibration at 34 GHz, there is still a significant uncertainty in the measurement of 34 GHz power levels. These sources of error may account for the order of magnitude difference between theory and experiment at 34 GHz.

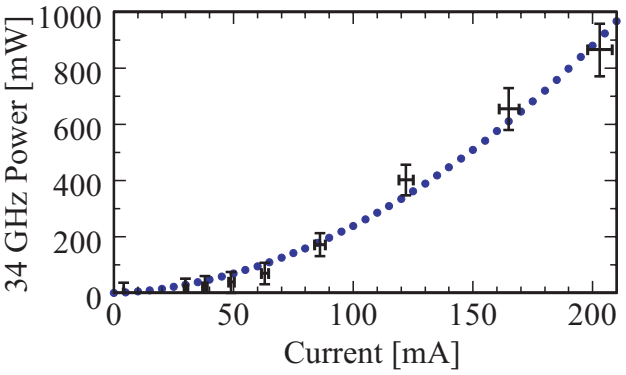

Figure 7: Power observed on output port with matched input port, at 34 GHz, versus current. Quadratic fit to data shown in blue dotted line with data given as black bars.

Power measurements were also made using the horn and diode detector combination shown in Fig. 2, detecting through the vacuum chamber window. Peak values observed over a scan in detector position for 100 mA average beam current were: 21 mW at 17 GHz, and 240 mW at 34 GHz. Discrete peaks were observed radiated from each of the six cells.

Wakefield measurements were also made as a function of the beam displacement from the axis. The 1.3 mm beam size, and 3.5 mm input collimator diameter gave a reasonable range of position variation. Results proved to be entirely attributable to beam current loss as the beam was intercepted by the input collimator. Current transmitted through the structure varied as would be expected when a 1.3 mm Gaussian profile is passed through a 3.5 mm aperture. After normalizing for beam current variations, the results of observations made with the Ku-band diode were unchanged as a function of beam offset. As expected, the loss factor for the fundamental does not vary with offset position. Observations in the Ka-band similarly show only dependence on the total current through the structure, and little variation with beam offset alone. This result is also expected, given the field pattern of the 34 GHz mode of Fig. 4.

Heterodyne frequency measurements were made, and peaks were only observed at integer multiples of the linac rf frequency f_{rf}, 17.14 GHz. A summary of observed frequencies is given in Table 5. To make the harmonic signal measurements possible, a length of Ka-band waveguide was used to filter the 17.14 GHz signal. No clear signal was observed of the dipole HOMs of the PBG structure, such as the 23 GHz mode of Fig. 4. The heterodyne detector has very high sensitivity to narrow band power, but cannot measure absolute scale power. The power detected at frequencies above 34.28 GHz with the heterodyne system was not observable with diode detectors. HOMs were only observed at multiples of f_{rf}.

Frequency [GHz]	f_{rf} multiple
17.14	1
34.28	2
51.42	3
68.56	4
85.7	5

Table 5: Heterodyne receiver observations in GHz, and corresponding integer multiple of f_{rf}, 17.14 GHz.

Wavemeters were used across K-band to look for signs of other HOMs. Modes were observed in agreement with heterodyne measurements; integer harmonics of f_{rf} were observed, no other HOMs were. Waveguide cutoff frequencies were exploited to filter unwanted 17 GHz wakes from power measurements in other bands, or near other frequencies when signals of HOMs were being sought. An adjustable narrow band pass filter was tuned to 34 GHz, with flat transmission within ~1 GHz, and used to verify that all power detected in the 26–40 GHz band was in fact at 34.28 GHz, or twice f_{rf}.

4. Discussion and Conclusion

Excellent agreement is seen between experimental measurements and theoretical predictions for wakefield power at 17 GHz. This agreement serves as a benchmark for the *ANALYST* wakefield simulation results. Wakefield simulation calculations using *ANALYST* predict more power in HOMs than is observed in experiments, by an order of magnitude. Minor variations between the experiment and simulations may be at fault, but the more likely cause is that the inherent measurement of low power in a high background environment is only capable of order of magnitude accuracy.

Excellent agreement is seen between experimental measurements and theoretical predictions for wakefield power at 17 GHz. This agreement serves as a benchmark for the *ANALYST* wakefield simulation results. Wakefield simulation calculations of higher order modes using *ANALYST* predict more power at 34 GHz than is observed in experiments, by an order of magnitude. The most likely cause of this discrepancy is difficulty in estimating the efficiency of transmission of the 34 GHz power in traveling from the structure through overmoded waveguide and a window to the detector. The scaling of wakefield power with current was measured at both 17 and 34 GHz and was found to scale quadratically, as expected from theory. The power in HOMs at 34 GHz is poorly confined in the transverse direction and leaks directly out of the photonic structure transversely; that power was experimentally detected through a quartz window using a horn and diode detector. HOMs at higher harmonics, up to the fifth harmonic at 85 GHz, could be observed with a heterodyne receiver system, although the power in harmonics above the second could not be accurately measured.

The quality factor ratios calculated in Sec. 2.3, while not directly capable of predicting power levels, provide a great deal of insight as to where the power lost by the beam can be expected. At 17 GHz a traveling wave mode is generated, and

very little power is lost due to diffraction out of the PBG lattice. At 34 GHz, diffractive loss dominates, and power is expected to leak out the open outer wall of the structure. Diffractive loss is so dominant that equal power is experimentally observed in port and chamber measurements. This should not be surprising, as power measured on the port is only that lost by the beam in the coupling cell directly attached to the port.

This paper has demonstrated both theoretically and experimentally that HOMs exist in PBG accelerator structures, and are not simulation artifacts. Theoretical work has identified the mode patterns expected, and that the mode quality factors, Q_n, serve as a quantitative figure of merit to identify HOM damping in PBG structures. Future design work can focus on what Qs are achievable in PBG structures, and how these numbers compare to other damping techniques. Cold test measurements, as in Fig. 5, showed dramatic HOM damping improvement by adding an external damping material, and this process can be extended to make damping in PBG structures more effective.

5. Acknowledgements

This work was supported by the Department of Energy, Division of High Energy Physics Contract No. DE-FG02-91ER40648. The authors gratefully acknowledge useful discussions with Jake Haimson, Amit Kesar, Cho Ng, and Kwok Ko; and experiment support from Ivan Mastovsky, Brian Munroe, and Emilio Nanni.

References

[1] D. R. Smith, N. Kroll, and S. Schultz, in Proceedings of the 1995 Advanced Accelerator Concepts: Sixth Workshop, AIP Conf. Proc. No. 335 (1995), pp.761–776.

[2] M. A. Shapiro, W. J. Brown, C. Chen, J. R. Sirigiri, E. I. Smirnova, and R. J. Temkin, in Proceedings of the 2001 Particle Accelerator Conference, (IEEE, Piscataway, NJ, 2001), pp. 930–932.

[3] E. I. Smirnova, I. Mastovsky, M. A. Shapiro, R. J. Temkin, L. M. Earley, and R. L. Edwards, Phys. Rev. ST Accel. Beams **8**, 091302 (2005).

[4] E. I. Smirnova, A. S. Kesar, I. Mastovsky, M. A. Shapiro, and R. J. Temkin, Phys. Rev. Lett. **95**, 074801 (2005).

[5] R. D. Ruth, in Proceedings of the 1996 European Particle Accelerator Conference, Barcelona, Spain, (1996), pp. 47–51.

[6] Y. H. Chin, N. Akasaka, Y. Takeuchi, K. Tajima, and C. K. Ng, in Proceedings of the 1996 European Particle Accelerator Conference, Barcelona, Spain, (1996), pp. 2000–2002.

[7] A. Grudiev, and W. Wuensch, in Proceedings of LINAC 2004, Lubeck, Germany, (2004), pp. 779–781

[8] B. Aune et al., Phys. Rev. ST Accel. Beams **3**, 092001 (2000).

[9] T. Shintake, Jpn. J. Appl. Phys. Vol. 31, Part2, No.11A, pp. L1567–L1570, 1992.

[10] S. Schultz, D. R. Smith, and N. Kroll, in Proceedings of the 1993 Particle Accelerator Conference, (IEEE, Piscataway, NJ, 1993), pp. 2559–2563.

[11] N. Baboi, R. M. Jones, G. B. Bowden, V. Dolgashev, S. G. Tantawi and J. W. Wang, in Proceeding of the 2002 European Particle Accelerator Conference, Paris, France, (2002), pp. 1440–1442.

[12] J. G. Power, M. E. Conde, W. Gai, R. Konecny, P. Schoessow, and A. D. Kanareykin, Phys. Rev. ST Accel. Beams **3**, 101302 (2000).

[13] R. A. Marsh, M. A. Shapiro, and R. J. Temkin, in Proceedings of the 2008 European Particle Accelerator Conference, Genoa, Italy, (2008), pp. 2841–2843.

[14] C. Adolphsen, K. Bane, T. Higo, K. Kubo, R. Miller, R. Ruth, K. Thompson, and J. Wang, Phys. Rev. Lett. **74**, 2475–2478 (1995).

[15] T. Wangler, Principles of RF Linear Accelerators, John Wiley & Sons, Inc., New York, 1998.

[16] R. A. Marsh, M. A. Shapiro, E. I. Smirnova, and R. J. Temkin, in Proceedings of the 2007 Particle Accelerator Conference, (IEEE, Piscataway, NJ, 2007), pp. 3002–3004.

[17] R. A. Marsh, M. A. Shapiro, and R. J. Temkin, in Proceedings of the 2007 Particle Accelerator Conference, (IEEE, Piscataway, NJ, 2007), pp. 3005–3007.

[18] I. Gonin, N. Solyak, J. DeFord, B. Held, in Proceedings of the 2007 Particle Accelerator Conference, (IEEE, Piscataway, NJ, 2007), pp. 2248–2250.

[19] J. DeFord, B. Held, J. J. Petillo, in Proceedings of the 2007 Particle Accelerator Conference, (IEEE, Piscataway, NJ, 2007), pp. 3600–3602.

[20] N. Kroll, S. Schultz, D. R. Smith, and D. C. Vier, in Proceedings of the 1999 Particle Accelerator Conference, (IEEE, Piscataway, NJ, 1999), pp. 830–832.

[21] W. J. Mulligan, S. C. Chen, G. Bekefi, B. G. Danly, and R. J. Temkin, IEEE Trans. Electron Devices **38**, 817 (1991).

[22] J. Haimson, B. Mecklenburg, G. Stowell, K. E. Kreischer, and I. Mastovsky, in Proceedings of the 1999 Conference on High Energy Density Microwaves, AIP Conf. Proc. No. 474 (AIP, New York, 1999), p. 137.

[23] J. Haimson, B. Mecklenburg, in Proceedings of the 1995 Particle Accelerator Conference (IEEE, Piscataway, New Jersey, 1995), pp. 755–757.

[24] J. Haimson, B. Mecklenburg, G. Stowell, and B. Ishii, in Proceedings of the 2002 Advanced Accelerator Concepts: Tenth Workshop AIP Conf. Proc. No. 647 (AIP, New York, 2002), pp. 810–820.

[25] J. Haimson, in Proceedings of the 2004 Advanced Accelerator Concepts: Eleventh Workshop AIP Conf. Proc. No. 737 (AIP, New York, 2004), pp. 95–108.